ACS Photonics

Article

pubs.acs.org/journal/apchd5

Atomistic Quantum Plasmonics of Gold Nanowire Arrays

Luca Sementa,[†] Andrea Marini,[‡] Giovanni Barcaro,[†] Fabio R. Negreiros,[†] and Alessandro Fortunelli*[,†]

[†]CNR-ICCOM and IPCF, Consiglio Nazionale delle Ricerche, v. G. Moruzzi 1, I-56124 Pisa, Italy

[‡]CNR-ISM, Consiglio Nazionale delle Ricerche, v. Salaria Km 29.5, I-00016 Monterotondo, Italy

Supporting Information

ABSTRACT: The dielectric properties of a regular 2D array of Au nanowires are investigated using time-dependent density-functional theory employing a fully atomistic quantum description. Longitudinal modes produce a Drude-like peak in the infrared that is rather insensitive to geometrical parameters. Transverse modes, instead, give rise to a plasmonic peak in the optical region, which exhibits a nontrivial dependence on the spatial separation between the wires: a strong resonant enhancement and a shift from the optical to the far-infrared region is observed as the interwire distance is decreased, with the formation of "hot spots" in which induced field and charge distributions exhibit nondipolar shape and rapidly alternating quantum phase. The general character of this phenomenon is confirmed by its occurrence in Au nanoparticle arrays. Addition of ligand species in the hot spot region can lead to the appearance of new resonances due to strong coupling between plasmonic and molecular modes, as exemplified in a proof-of-concept case. This shows the possibilities of atomistic quantum plasmonics effects and subwavelength control of electromagnetic field intensity in properly engineered nanogaps.

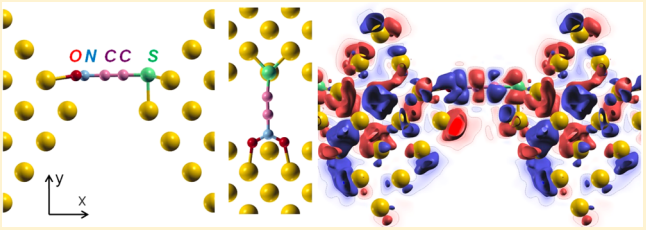

KEYWORDS: *time-dependent density-functional theory, optical response, macroscopic dielectric function, molecule/plasmon coupling, single-molecule detection, nanogaps*

The synthesis of new materials at the nanometer scale has strongly developed in recent years, due to continuous advances that allow one to manipulate matter at an unprecedented level of precision, thus creating a diverse set of nano-objects with controlled size, shape, and chemical environment, as well as relative arrangement.[1] Among these, metallic nanowires[2−5] exhibit unique optical properties due to the bipolar character of their optical spectrum, which—combining longitudinal modes akin to bulk excitations with transverse modes resembling those of finite nanostructures—offers an increased freedom in applications. Longitudinal modes can be exploited, e.g., in opto-electronic devices (wave-guiding light at deep-subwavelength scales over micrometric distances[6]) and in life science as diagnostic imaging and therapeutic (cancer) agents,[7] as well as in sensing.[8] Transverse modes fall in the general theme of confined metallic resonances and can also be utilized in theranostics as well as sensing. The electromagnetic field enhancement in the proximity of the wires and its high sensitivity to nearby microscopic objects afford great sensing capabilities, such as in surface-enhanced Raman scattering (SERS) and surface-enhanced infrared absorption (SEIRA),[9,10] especially when metallic structures interact synergistically to produce "hot spots" in the so-called field of "plasmonics",[11−13] in which the ultimate goal of single-molecule detection and recognition is eventually approached. In this context, one of the most interesting and so far little investigated phenomena takes place in the case of nearly touching metallic nanostructures, possibly intermixed with organic species, in which the short-range physics of the system (rather than the long-range behavior as it often happens in optics) is sampled.[14] Such short-range plasmonic phenomena in properly engineered nanogaps depend critically on the spatial profile and spectrum of near electric fields relative to the resonances and local configuration of the molecules in a narrow nanometer-scale interwire region.[15] To fully understand and predict these, theoretical tools are required that achieve an atomistic quantum description. Beyond a certain level of coarseness introduced by atomic length scales, in fact, quantum mechanical effects and the atomistic grain of the system simultaneously acquire a decisive role, and current semi-classical[13] or jellium electron-gas[16,17] models, which are able to predict (under appropriate conditions in an even quantitatively precise way) the long-range behavior of induced fields but in which the quantum and/or the atomistic levels of description are lacking, become inaccurate.[18]

Here we tackle such a problem and show that it is possible to predict the optical properties of a regular array of Au nanowires and their plasmonic resonances[17] via a fully quantum-mechanical description, providing the exact microscopic shape of the system response functions. As a crucial point, the method retains its predictive character when the nanowires approach each other: We are thus able to investigate the strong enhancement of the induced electromagnetic field in atomic-scale hot spots created in the case of subnanometer nanowire

Received: August 19, 2013
Published: March 20, 2014

separations and to prove that its spatial and phase profiles exhibit nontrivial atomistic quantum features that can hardly be described using lower-level theoretical approaches. Knowledge of these profiles then guides us in the design of a proof-of-principle example in which the introduction of a docking molecule in the hot spot region gives rise to novel absorption peaks and intense resonances due to the strong coupling between plasmonic and molecular modes, hence illustrating the kind of fascinating possibilities thus opened. This widens our predictive understanding of plasmonics effects at the sub-nanometer scale and their subwavelength control.[19]

METHODS

An atomistic model of a realistic nanowire or nanorod entails a huge amount of atoms, which makes first-principles simulations practically unfeasible. Since these systems are characterized by one spatial dimension much bigger than the other two, we use periodic boundary conditions to set up 1D models with a limited number of atoms per unit cell, still preserving the main features of the real systems. Au nanowires of different cross sections, with 36 up to 58 atoms per unit cell, are considered, with fcc structure and grown along a (110) direction in the z-axis, mimicking systems 1−3 nm in diameter and replicated in a 2D periodic array (see Figure 1 for an array of a Au nanowire

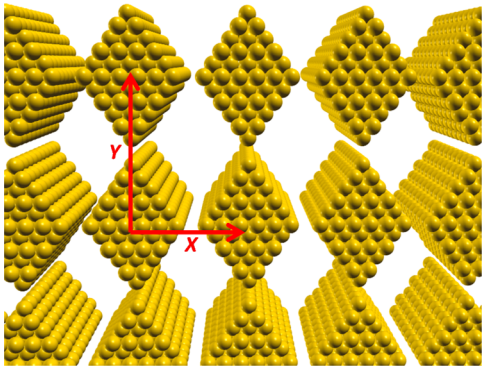

Figure 1. Schematic picture of the 2D array of Au nanowires studied in the present work. The unit cell measures (25.0, 30.5, 2.88) Å in the (x, y, z) directions. For clarity, a few unit cells along the nanowire main (z-)axis direction are shown. The total dimensions of the figure are (100.0, 76.25, 28.8) Å.

with a 36-atom unit cell). We can calculate only the longitudinal central mode and not the end modes specific for finite nanorods[15,18] due to the periodic boundary conditions. However, an advantage of the present periodic approach is that the interwire separation can be varied without increasing the computational effort and used to investigate the whole range of nanowire/nanowire interactions from negligible to strong plasmonics effects: distances between atoms in replicated cells ranging from 5 to 15 Å are sufficient for this purpose.

First-principles calculations are performed employing two computational packages, Abinit[20] and Yambo,[21] with the former used to generate the electronic ground state and a number of virtual monoelectronic states via density-functional theory (DFT) in the local density approximation (LDA) and the latter used to calculate the macroscopic dielectric function $\varepsilon(\omega)$ of the system in the linear response regime, via the time-dependent version of density-functional theory (TDDFT). The absorption spectra is given by the imaginary part of the $\varepsilon(\omega)$:

$$\varepsilon(\omega) = \left[1 + \lim_{q\to 0} \frac{4\pi}{|q|^2}\chi_{G,G'}(q,\omega)\right]^{-1}_{G=0,G'=0} \quad (1)$$

where ω and q are the frequency and wave vector of the electromagnetic field, respectively, and $\chi_{G,G'}(q,\omega)$ is the polarizability of the real electronic system that is obtained from the Kohn−Sham independent-particle polarizability $\chi^0_{G,G'}(q,\omega)$ by solving the equation[22]

$$\chi_{G,G'}(q,\omega) = \chi^0_{G,G'}(q,\omega) + \sum_{G_1,G_2} \chi^0_{G,G_1}(q,\omega) \left(\frac{4\pi}{|q+G_1|^2}\delta_{G_1,G_2} + f^{xc}_{G_1,G_2}(\omega)\right)\chi_{G_2,G'}(q,\omega) \quad (2)$$

where $f^{xc}_{G_1,G_2}(\omega)$ is the exchange−correlation kernel here assumed in (adiabatic) LDA form. The use of LDA for deriving the band structure and the kernel of linear response yields semiquantitatively correct results, although the absorption peaks are red-shifted with respect to more sophisticated but more computationally demanding exchange−correlation functionals,[23] which will be considered in future work. In the literature, atomistic TDDFT calculations have been performed on finite clusters with a large aspect ratio[24−26] or on infinite monatomic chains.[27] In both cases, transverse cross sections are extremely limited with respect to the present approach and the real systems.

Numerical convergence is tested with respect to numerical parameters of the calculations: a grid of (1, 1, 40) k-points is used (validated with tests using up to 80 k-points in the z-direction); the number of pairs of G vectors is 2.5×10^5 (validated with tests using up to 10^6 pairs of G vectors); 40 au is used as the energy cutoff for the selection of the plane wave basis set for the description of the wave function (validated with tests using a cutoff up to 60 au). In order to avoid numerical problems due to vanishing energy denominators, interband and intraband contributions to the dielectric function are evaluated separately. Interband contributions are calculated from eqs 1 and 2 by neglecting transitions with equal band indexes in the formula of the $\chi^0_{G,G'}(q,\omega)$ polarizability. Intraband contributions correspond to the Drude components of $\varepsilon(\omega)$, which for a metallic system give $\mathrm{Re}[\varepsilon](\omega) \approx (1 - \omega_0^2/\omega^2)$ and $\mathrm{Im}[\varepsilon](\omega) \approx \omega_0^2\tau/(\omega_0^2\tau + 1)\cdot 1/\omega$,[28] where Re[] and Im[] are real and imaginary parts, respectively, ω_0 is the plasmon frequency, and τ is an effective relaxation time. Intraband contributions are separately evaluated by using in eqs 1 and 2 a small value of $|q| = 0.0125$ (which is sufficiently large to avoid numerical divergences but sufficiently small to be treated as a perturbation) and restricting the calculation of the $\chi^0_{G,G'}(q,\omega)$ polarizability only to the semioccupied bands (i.e., those crossing the Fermi energy) and added to $\varepsilon(\omega)$ as *a posteriori* corrections.

Apart from the dielectric function $\varepsilon(\omega)$, a fundamental quantity to connect TDDFT calculations with experimental measurements is the induced electron charge density (or equivalently the related quantity: the induced electric field). Within linear response theory, the induced electron charge density $\rho_{ind}(\mathbf{r},\omega)$ due to an external field of frequency ω is given by $\rho_{ind}(\mathbf{r},\omega) = \int\chi(\mathbf{r};\mathbf{r}',\omega)\,\phi_{ext}(\mathbf{r}',\omega)\,d\mathbf{r}' = \int\chi^0(\mathbf{r};\mathbf{r}',\omega)\,\phi_{tot}(\mathbf{r}',\omega)\,d\mathbf{r}'$, where the total self-consistent potential $\phi_{tot}(\mathbf{r}',\omega)$ is the sum of the external and induced potential: $\phi_{tot}(\mathbf{r}',\omega) = \phi_{ext}(\mathbf{r}',\omega) + \phi_{ind}(\mathbf{r}',\omega)$, and $\chi(\mathbf{r};\mathbf{r}',\omega)$ is the nonlocal

dx.doi.org/10.1021/ph500038z | ACS Photonics 2014, 1, 315−322

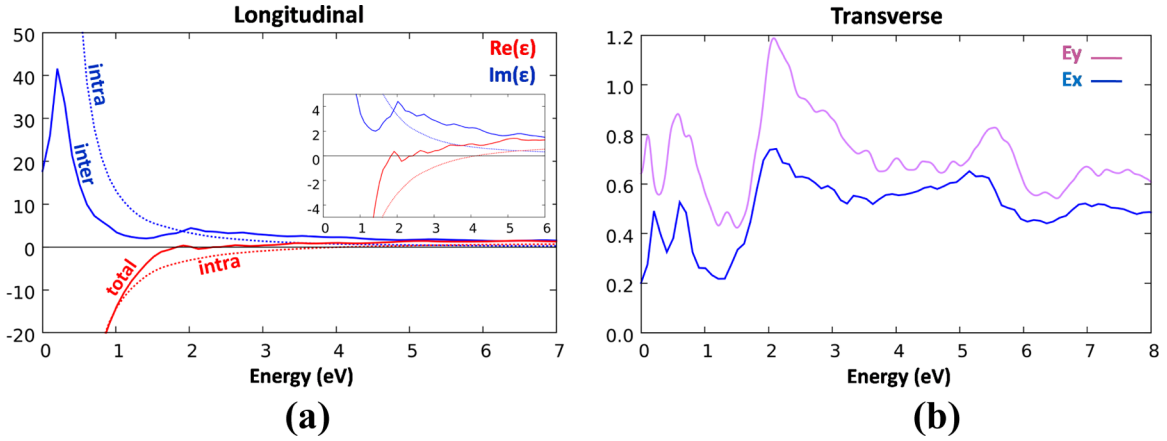

Figure 2. Plots of the macroscopic dielectric function $\varepsilon(\omega)$ for the 36-atom Au nanowire system: (a) real [Re(ε)] and imaginary [Im(ε)] parts of $\varepsilon(\omega)$ in the longitudinal direction distinguished as intraband (intra), interband (inter), and total contributions; in the inset the region where the red curves cross the energy axis is zoomed in; (b) imaginary parts in the transverse x (Ex) and y (Ey) directions. Interwire separation is such that distances between atoms in replicated cells are at least 10 Å.

density−density response function.[18] In order to evaluate $\rho_{ind}(\mathbf{r}, \omega)$, we project $\chi(\mathbf{r}; \mathbf{r}', \omega)$ on the basis of LDA Bloch electron−hole pair functions:

$$\chi(r, r', \omega) = \sum_{\alpha_1,\beta_1,\alpha_2\beta_2} \phi^*_{\alpha_1}(r)\, \phi_{\beta_1}(r)\, \chi^{\alpha_1,\beta_1}_{\alpha_2,\beta_2} \phi^*_{\alpha_2}(r')\, \phi_{\beta_2}(r') \tag{3}$$

and we calculate the coefficients $\chi^{\alpha_1,\beta_1}_{\alpha_2,\beta_2}$ searching for the poles of $\chi(r, r', \omega)$.[29] As we are interested in the induced density with ω in the infrared, to evaluate $\rho_{ind}(\mathbf{r}, \omega)$, we limit electron−hole pair functions to those with excitation energy less than 4 eV and consider a smaller set of k-points (10) than that used to solve eq 2. In the following for definiteness we only consider $\rho_{ind}(\mathbf{r}, \omega)$, but the corresponding plots can be easily transformed into plots of induced or total mean-field potential or electric field via the formulas given above.

RESULTS AND DISCUSSION

Let us start by briefly discussing the dielectric response of independent nanowires. In Figure 2, the spectral response of the nanowire system of Figure 1 is reported for a value of interwire separation large enough that nanowire/nanowire interactions are basically negligible. The plots show the real (Re[ε] or ε_1) and imaginary (Im[ε] or ε_2) components of the macroscopic dielectric response function as a function of the electromagnetic field frequency (ω). As anticipated above, free-charge-carrier (plasmon-like) excitations in nanowires give rise to two coexisting but well-separated absorption bands:[30,31,5] a long-wavelength band in the infrared region resulting from the longitudinal oscillation of the conduction band electrons, and a short-wavelength band corresponding to the electronic oscillations in the transverse directions. Longitudinal and transverse components are separately reported in Figure 2.

In the longitudinal component (Figure 2a) intra- and interband contributions are distinguished. It can be noted that the intraband contribution to $\varepsilon_1(\omega)$ crosses the ($\varepsilon_1 = 0$) axis at around 4. eV, i.e., at a frequency smaller by a factor ∼2 than in the bulk (real and imaginary parts of the macroscopic dielectric function of wires of different size and for bulk fcc Au; also local field effects and the nonlocal part of the pseudopotential and as a function of interwire separation, are provided in the Supporting Information (SI)), in agreement with the expected lowering of the plasmon frequency ω_0 in passing from 3D to 1D systems.[32] However, after adding the interband contribution the total $\varepsilon_1(\omega)$ crosses the ($\varepsilon_1 = 0$) axis in a region where $\varepsilon_2(\omega)$ is appreciably different from zero so that no plasmonic peak is eventually expected in the EELS response of the present nanowires. In passing, it can be mentioned, as shown in more detail in the SI, that the longitudinal response is basically not influenced by local-field effects, i.e., effects going beyond single-particle approximation, confirming its free-electron, Drude-like, and long-range character.

In contrast with the longitudinal component, the real part $\varepsilon_1(\omega)$ of the transverse dielectric function exhibits a pronounced peak close to 2 eV (thus quite different from 0-axis crossing), as shown in the SI. The transverse imaginary part $\varepsilon_2(\omega)$ also exhibits a clear peak slightly above ∼2 eV = 600 nm. This can be put into a straightforward correspondence with the absorption spectrum of 0D finite nanoparticles exhibiting similar cross-section:[23] the good agreement with the theoretical predictions on the latter systems, which—after correcting for effects due to the choice of the xc-functional and the external environment—are also in good agreement with experimental data,[23] validates the accuracy of the present approach (we have indeed applied the present approach also to selected finite clusters and again found an excellent agreement with the results of ref 23, not shown). This is a crucial point also in view of the significance of the present results and the connection between the predicted dielectric response of regular arrays of ultrasmall Au wires and the current experimental state of the art (i.e., real experimental situation). The straightforward correspondence between the optical response of nanoparticles and the transverse mode of infinite nanowires exhibiting the same cross-section indicates that such modes really possess a *local* character with respect to directions orthogonal to the exciting electric field and only depend on the confined and surface-modulated oscillations of quasi-free metal electrons along the direction of the field. It is thus possible to use nanowires as models of nanostructures without worrying about the difference between the nanowire regular ("perfect") arrangements along their axis and the finiteness of nanoparticles. Assuming perfect translational periodicity as in our models is only very advantageous because of technical (computational) reasons. The wires shown in Figure S1 of the SI, for example, can be put

dx.doi.org/10.1021/ph500038z | ACS Photonics 2014, 1, 315−322

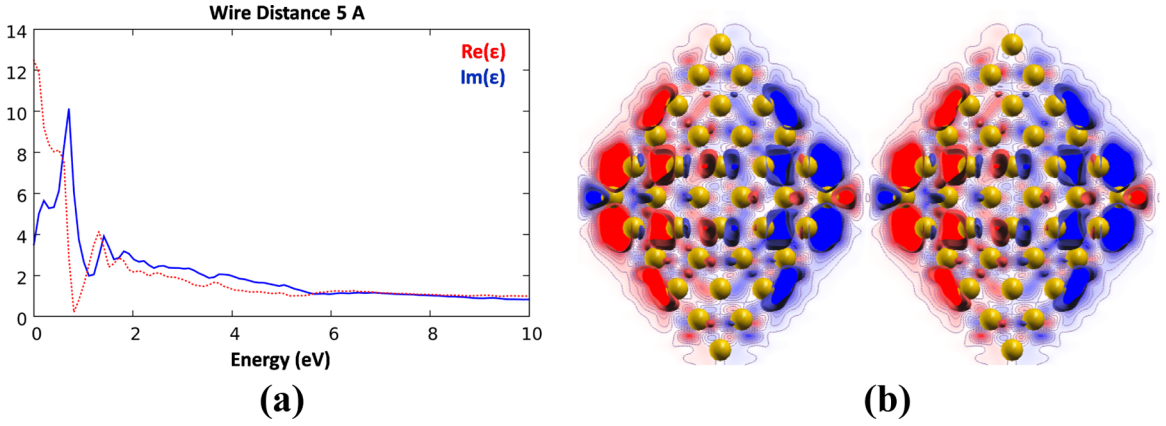

Figure 3. (a) Real [Re(ε)] and imaginary [Im(ε)] parts of the transverse component of the macroscopic dielectric function $\varepsilon(\omega)$ for the 36-atom nanowire array. (b) Isocontours (values = $\pm 2 \times 10^{-3}$ electrons Å^{-3} for an electric field of 1 V/nm) of $\rho_{ind}(\mathbf{r}, \omega)$ related to the highest transverse peak of the 36-atom nanowire at ω = 0.707 eV. The nanowire separation (minimum distance between atoms in replicated cells) along the x-axis is 5 Å.

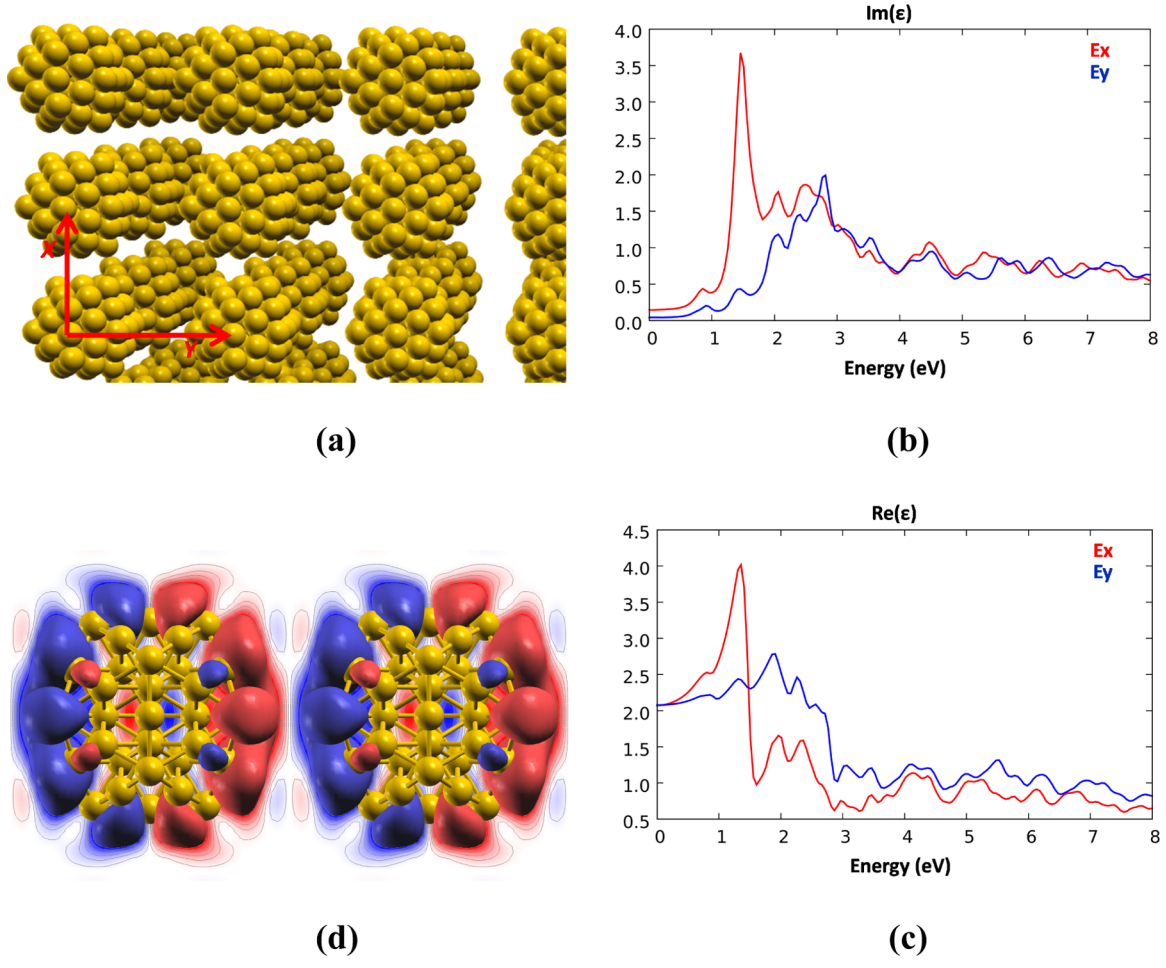

Figure 4. (a) Pictorial view of a 3D array of Au nanoparticles: the interparticle separation is 5 Å along the x-direction and 9.5 Å along the y-direction; (b) imaginary [Im(ε)] and (c) real [Re(ε)] parts of the macroscopic dielectric function along the x- and y-directions; (d) isocontours (values = $\pm 2 \times 10^{-3}$ electrons Å^{-3} for an electric field of 1 V/nm) of $\rho_{ind}(\mathbf{r}, \omega)$ related to the peak in [Im(ε)] at ω = 1.52 eV for the electric field oriented along the x-direction. The unit cell in (a) measures (14.5, 19.0, 19.0) Å in the (x, y, z) directions. For clarity, a few unit cells along the three Cartesian directions are shown, so that the total dimensions of the figure are (43.5, 66.5, 57.0) Å.

in correspondence with truncated octahedral clusters as follows: W(36) = TO(6,0)$_{146}$, W(37) = TO(7,3)$_{147}$, W(47) = TO(7,1)$_{225}$, W(58) = TO(8,2)$_{314}$, W(69) = TO(9,3)$_{405}$, where W(N) is the N-atom wire and TO(L,P)$_M$ is a M-atom truncated octahedron with L-atom side and a P-atom truncation of its six (100) vertexes. We underline that in this respect nanowire modeling allows us to consider rather large sizes: a nanowire with a cross-section of 36 atoms corresponds to a 146-atom nanoparticle, while a nanowire with a cross-section of 69 atoms corresponds to a 405-atom nanoparticle.

dx.doi.org/10.1021/ph500038z | ACS Photonics 2014, 1, 315−322

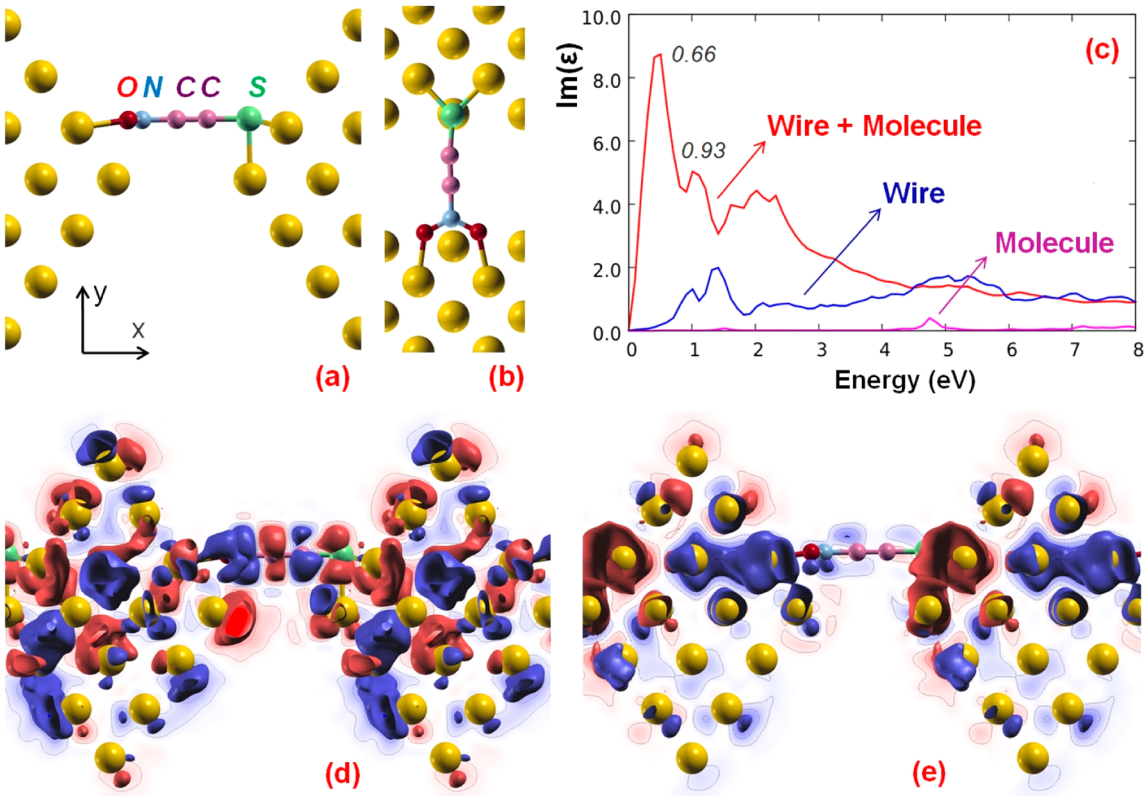

Figure 5. Side (a) and top (b) pictorial views of the unit cell of a 2D array of 16-atom Au nanowires interconnected by a $SCCNO_2$ molecule: the interparticle separation is 5.4 Å along the *x*-direction and 10.0 Å along the *y*-direction. (c) Imaginary [Im(ε)] part ("Molecule + Wire" in red) of the macroscopic dielectric function along the *x*-direction for the system in (a) and (b) compared with the same quantity calculated for systems in which only the wire ("Wire", in blue) or the neutral molecule ("Molecule" in magenta) is present in the cell. (d, e) Isocontours (values = $\pm 2 \times 10^{-3}$ electrons $Å^{-3}$ for an electric field of 1 V/nm) of $\rho_{ind}(\mathbf{r}, \omega)$ related to the peaks in [Im(ε)] shown in (c) at ω = 0.66 eV and 0.93 eV, respectively, for the electric field oriented along the *x*-direction. The unit cell in (a) and (b) measures (14.1, 22.2, 5.76) Å in the (*x*, *y*, *z*) directions.

Defects and inhomogeneities that are likely to be present in the experimental nanowire will thus not be relevant to their transverse response or, better, will be only *locally* relevant.

We now focus on the dielectric response of the nanowire array as a function of interwire separation and deform the periodic lattice by keeping the interwire distance along the *y*-axis fixed and decreasing the distance along the *x*-axis. The longitudinal response does not present particular surprises: the positions of the main peaks in both the real and imaginary components do not change with the distance between the wires, while their intensity and overall integral scale with the cell volume, in keeping with general expectations (see the SI). A completely different behavior is exhibited by the transverse $\varepsilon(\omega)$, reported in Figure 3a for an an interwire separation along the *x*-axis of 5 Å (further plots are reported in the SI). We find in fact that at a given frequency (around 0.7 eV for the 36-atom nanowire array) simultaneously Re[ε](ω) goes to zero and a new very strong absorption peak develops in Im[ε](ω). The intensity of this peak is larger by more than an order of magnitude than the corresponding adsorption intensity at great interwire separations, therefore corresponding to a true plasmonic effect. Moreover, its peak position and intensity are in good agreement with experiment.[33]

To further analyze this plasmonic resonance, in Figure 3b we show the induced density $\rho_{ind}(\mathbf{r}, \omega)$ at the peak frequency (ω = 0.707 eV). First, the atomistic grain of $\rho_{ind}(\mathbf{r}, \omega)$ in the transverse case can be contrasted with the long-range character of the free-electron-like peak in the longitudinal response shown in the SI. Second, the dipolar character of the transverse excitation is immediately apparent, but what is also apparent and is nontrivial is the atomistic grain of the wave function phase at the tips or edges of the wires, where regions of positive and negative phase alternate in a subtle yet atomistically precise manner. Higher-order deformations such as quadrupolar components are predicted by electrodynamic models in the limit of nearly touching systems,[16,34,36] but to go beyond such qualitative expectations and achieve a precise description at short distances from the nanostructure surface, a fully atomistic quantum mechanical calculation such as the present one is required. These fine details can be crucial in applications such as SERS, because the electric field generated by the metal resonance, its enhancement in the plasmonic régime, and its interaction with the molecular oscillator strengths of the Raman-active molecules docked onto the nanoparticles have profound effects on the system's sensing capabilities.[37] The question can be asked whether this plasmonic resonance has bearings on the charge transfer mode discussed in previous jellium-based studies.[16] A deeper analysis of the induced current across the junction would be needed to answer this question. However, it seems to us that the distance between the edges of the wires is not sufficient to induce transport effects and real hybridization: in Figure 3b no great physical overlap between the induced electron densities on neighboring nanowires is apparent.

This plasmonic phenomenon has a general character, as proven by its appearance in embryonic form in smaller, finite-

size systems. Let us in fact "break" the wires along the z-axis, thus obtaining a 3D array of Au nanoparticles arranged at the centers of a cubic lattice, as shown in Figure 4a (in detail, icosahedral Au_{55} particles are here considered). In analogy with the nanowire case, we can define the lattice in such a way that one of the sides—the x-axis—is shorter than the other two, so that the distance between closest atoms in the x-direction is 5 Å, whereas it is 10 Å in the y- and z-directions. By comparing the plots of $\mathrm{Im}[\varepsilon](\omega)$ in the x- and y-directions in Figure 4b, we see that in the direction of closest approach (the x-axis) but *not* in the orthogonal y-direction, for an interwire distance smaller than the nanoparticle size, a neat plasmonic peak arising from nanoparticle−nanoparticle interactions[33] develops at a frequency ω around 1.5 eV. This peak is of lesser intensity and is less red-shifted with respect to that of the nanowire system shown in Figure 3a due to the smaller, molecular-like size of the Au_{55} nanoparticles, but is still clearly present. It can be noted (see Figure 4c) that, in correspondence with the peak in $\mathrm{Im}[\varepsilon](\omega)$, the real part $\mathrm{Re}[\varepsilon](\omega)$ of the dielectric function exhibits a dip that approaches the $\mathrm{Re}[\varepsilon] = 0$ axis (even though without crossing it), thus amplifying the EELS response of the system in perfect analogy with the nanowire case of Figure 3a. It is also instructive to analyze the nature of the induced density corresponding to this peak: in Figure 4d we plot $\rho_{\mathrm{ind}}(\mathbf{r}, \omega)$ at the peak position ($\omega \approx 1.5$ eV) for the field aligned along the x-direction, whence one can appreciate its dipolar character, with however some apparent atomic grain quadrupolar components analogous to those found in the nanowire case, thus suggesting that the presence of rapidly alternating quantum phases in $\rho_{\mathrm{ind}}(\mathbf{r}, \omega)$—and thus correspondingly in $\phi_{\mathrm{ind}}(\mathbf{r}', \omega)$—observed for the nanowire case in Figure 3b has a general significance for plasmonics effects in the régime of close approach. It is useful to underline the significance of the results presented in Figure 4. If plasmonic effects can be observed in such small systems as Au_{55}, intermediate between the molecule-like behavior of subnanometer clusters and the fully developed Mie response of larger particles, and also suffering from damping of plasmon resonance due to the small 5d/6s gap of Au, they can be expected to have a ubiquitous presence in many conditions.

The embryonic presence of plasmonic effects also in ultrasmall nanostructures as those shown in Figure 4 allows us to go one step further and investigate with a limited computational effort what happens when real molecules are introduced into the nanogaps between the wires,[14] along the lines of the pioneering work of ref 37. We thus consider a smaller nanowire with a 16-atom cross-section, which corresponds to a nanoparticle of 44 atoms: W(16) = $TO(4,0)_{44}$; we double the unit cell in the z-direction so as to have enough room for inserting a ligand but avoiding overlaps with molecules in replicated images, also slightly enlarge the minimum distance between the edges of the nanowire in the x-direction to 5.4 Å (instead of 5.0 Å), and finally insert a $SCCNO_2$ molecule between the nanowires as shown in the schematic pictures of Figure 5a,b. The molecule is put at an appropriate y-height such that its end atoms appreciably interact with the Au atoms in the nanowire and are close enough to the maxima in the induced density shown in Figure 3b for the 36-atom wire; very similar peaks appear in the induced density of W(16), except that their intensity is attenuated by the smaller size of the wire and slightly larger interwire distance. Such a ligand, even though strongly simplified, is intended to mimic a push−pull chromophore with its sulfur and nitrate end-groups, which also have an appreciable affinity toward Au and occur in real ligands. However, we stress that here we do not investigate in detail the docking structural problem, so that our results will have a proof-of-principle flavor. On this system we apply the same TDDFT computational approach as used above for the bare nanowire systems. Numerical parameters of the calculations are as follows: a grid of (1, 1, 30) k-points (considering the doubling of the unit cell in the z-direction, this corresponds to 60 k-points above); the number of pairs of G vectors is 10^6; 60 au is used as the energy cutoff for the selection of the plane wave basis set for the description of the wave function.

The imaginary part of the dielectric function for the separate nanowire and neutral ligand systems so obtained is shown in Figure 5c. The molecule is considered in its neutral form because in our periodic approach we cannot use charged systems, even though when ligated to the metallic nanostructure the sulfur group will be charged to a $-S^-$ thiolate, but validation calculations with a different code indicate that charging does not qualitatively change the $SCCNO_2$ molecular spectrum. In the neutral form the spectrum exhibits a first excitation around 1.6 eV with negligible intensity and much higher peak at around 4.7 eV. The bare nanowire, instead, has two plasmonic-enhanced low-energy broad bands between 0.8 and 1.4 eV, which are analogous to the 0.707 eV peak of the 36-atom nanowire. The crucial point here is the substantial difference between the spectra of the isolated fragments and that of the composed nanowire + molecule system also shown in Figure 5c: in the latter, intensity is drawn at low energy and concentrates into two main peaks below 1 eV with maxima at around 0.66 and 0.93 eV. Figure 5d,e report the induced densities corresponding to these peaks and illustrate their physical components. The peak at 0.93 eV resembles a dipolar plasmonic resonance analogous to the one reported in Figure 3b for W(36) but which is now spatially compressed into the wire by the presence of the docking ligand and is also concentrated in the upper part of the wire (an analogous resonance concentrated in the lower part of the nanowire with a lesser intensity is also present, not shown): this can be vaguely compared with the phenomenon observed in ref 35 for thiolate-protected Au_{144} clusters. The peak at 0.66 eV is more interesting. It shows how the plasmonic oscillation of electrons in the metallic nanowire transfers into and strongly hybridizes with the conjugated π-system of the molecule, thus producing a new excitation in a very different region of the optical spectrum, of very high intensity and with substantial contributions from both fragment systems. Although here realized in a proof-of-concept example, this is precisely the expected effect in which the optical modes of the component systems mix and their strong coupling produces an amplified resonance to investigate which atomistic quantum approach such as the present one is probably inescapable. It seems that the plasmonics interaction between the metal nanostructures as investigated here intensifies this coupling and somewhat qualitatively changes its nature with respect to the pioneering work of ref 37, in which single metal nanoparticles interacting with single ligand molecules were considered and single excitations from the nanoparticle to the ligand were found to appear. Such novel, intense, and low-energy modes offer several possible applications. For example, they are expected to be very sensitive to geometrical parameters and thus to vibrations and thus are usable in SERS,[37] or one can think that they change so much the wave function of the ligand as to trigger its reactivity (photocatalysis), and so on. Other ligand adsorption

modes such as symmetrical docking onto the nanostructure edge can also be considered. Investigating such fascinating paths is deferred to future work.

Before concluding, it is useful to recapitulate the connection between the predicted dielectric response of regular arrays of small Au wires discussed in our work and the current experimental state of the art (i.e., real experimental situation). Concerning the longitudinal component of the dielectric function, our results show how this quantity is basically bulk-like and corresponds to the limit of wires of infinite length (or zero aspect ratio). As such, our longitudinal component is not strongly affected by the interwire distance. Our work thus provides a model limit that is relevant to real systems (nanorods of finite aspect ratio) depending on the given physical effect one is investigating. Clearly, experimentally observed end-modes (which are sensitive to interwire distance) are not predicted by our calculations.[15,18,24,27,25,26] However the present approach predicts the dielectric function of nanowires with a finite cross-section: as discussed above, this dielectric function is different from the bulk one and can be used in electrodynamical modeling instead of assuming it from other experiments, as is done in a customary protocol whose quantitative accuracy is uncertain. The main focus of this work is however the nanowire transverse response and its dependence on the interwire distance. In this respect, we underline two points: (i) The strong similarity between the optical response of nanoparticles and the transverse mode of infinite nanowires is a crucial point. It proves the *local* character of such modes with respect to directions orthogonal to the exciting electric field, so that it is possible to use nanowires as models of finite nanostructures and exploit their perfect translational periodicity as a computationally convenient tool, which enables us to consider sizes larger than those considered before. (ii) Our focus is on the régime of closely approaching nanowires. Again, our results are relevant not only for a perfect 2D array of regular nanowires, as the same effects occur in dimeric structures,[17,36] only reinforced here by the presence of more than one pair. Once more, the model periodic system is chosen in our approach for its computational advantages. One can wonder whether such an intrinsically metastable situation as nearly touching nanostructures can be experimentally realized. In real experiments the contact between the plasmonic nanoparticles may happen simultaneously in several places through the protruding atoms, so that statistical sampling techniques are probably needed to accurately predict such effects. However, we argue that robust close approaches can indeed be achieved if geometrical, steric, or kinetic constraints preclude particle agglomeration.[14] Not only this, we venture to hypothesize that such situations have actually been already more or less knowingly constructed in empirical devices and observed in the scientific literature in several cases; see, for example, Ag fragmented clusters embedded in He droplets.[33]

CONCLUSIONS

In summary, here we investigate the dielectric properties (real and imaginary components of the macroscopic dielectric function for both longitudinal and transverse alignment of the exciting field) of a regular 2D array of Au nanowires via a first-principles TDDFT approach, achieving an atomistic detail of description. These systems represent convenient models for studying the optical response of strongly anisotropic objects such as nanorods of great appeal in optical applications,[6,10] as well as that of finite 0D systems such as metallic nanoparticles inasmuch as their transverse modes are concerned. Our method allows us to study the electromagnetic response of such systems going beyond the commonly used semiempirical or electrodynamics models and to approach within a consistent computational framework and with a comparable computational effort the very interesting and so far little explored régime of nearly touching nanowires (interwire separation smaller than the nanowire diameter). At such short distances in properly engineered nanogaps, the atomistic grain of the wires acquires a decisive role. We are able to predict the anomalously large shifts and new plasmonic bands that thus emerge, to unveil their nature, and to analyze the spatial profile and resonance spectrum of near fields in the "hot spots" of the nanostructure array, showing that the response wave function phase assumes a peculiar, atomistically precise shape with a rapidly alternating phase in the proximity of sharp edges (or in general in the regions of closest approach) and that this phenomenon has a rather general character, appearing in embryonic form also in ultrasmall, preplasmonic nanostructures. As the electric field enhancement in the subnanometer hot spot regions encompassing ligand molecules depends critically on the local configuration of both the plasmonic resonance and the molecules,[15] precise information on this quantity as obtained via the present atomistic first-principles description is deemed necessary to achieve optimal control and design of short-range plasmonics effects[19] in improved, computationally designed refractive-index-based nanosensing,[8] single-molecule (including DNA) detection and recognition,[7,14] field-enhanced spectroscopy,[9,10] plasmon-enhanced photochemistry, and plasmonic wave guiding.[6] This is shown in a proof-of-principle case in which knowledge of the atomistic details of the surface plasmonic resonance guides the design of a ligand molecule and a docking mode, which produce a strong coupling between plasmonic and molecular excitations: new frequencies appear at low energy, some of which correspond to a modulation of the metallic resonance due to the confinement caused by ligand charge compression, whereas others are completely novel excitations (some of noteworthy intensity) in which electrons oscillate from one wire to the next through the molecule, thus being promising both in terms of sensing and in terms of triggering ligand reactivity.

ASSOCIATED CONTENT

Supporting Information

Real and imaginary parts of the macroscopic dielectric function of wires of different size and for bulk fcc Au. Also local field effects and the effect of the nonlocal part of the pseudopotential on the macroscopic dielectric function and its behavior as a function of interwire separation for the 36-atom nanowire system. This material is available free of charge via the Internet at http://pubs.acs.org.

AUTHOR INFORMATION

Corresponding Author

*E-mail: alessandro.fortunelli@cnr.it.

Notes

The authors declare no competing financial interest.

ACKNOWLEDGMENTS

A.F. acknowledges Michel Pellarin and Emmanuel Cottancin for useful discussions and suggestions. Financial support from the ERC-AG SEPON project is gratefully acknowledged. Most

calculations were performed within the ISCRA project PRINS at Cineca Supercomputing Center (Bologna, Italy).

REFERENCES

(1) Rycenga, M.; Cobley, C. M.; Zeng, J.; Li, W.; Moran, C. H.; Zhang, Q.; Qin, D.; Xia, Y. Controlling the synthesis and assembly of silver nanostructures for plasmonic applications. *Chem. Rev.* **2011**, *111*, 3669−3712.
(2) Link, S.; El-Sayed, M. A. Spectral properties and relaxation dynamics of surface plasmon electronic oscillations in gold and silver nanodots and nanorods. *J. Phys. Chem. B* **1999**, *103*, 8410−8426.
(3) Bose, S. M.; Longe, P. Collective excitations in quantum wires formed in mesoporous silica. *J. Phys.: Condens. Matt.* **2002**, *14*, 1915−1921.
(4) Murphy, C. J.; Sau, T. K.; Gole, A. M.; Orendorff, C. J.; Gao, J.; Gou, L.; Hunyadi, S. E.; Li, T. Anisotropic metal nanoparticles: synthesis, assembly, and optical applications. *J. Phys. Chem. B* **2005**, *109*, 13857−13870.
(5) Pérez-Juste, J.; Pastoriza-Santos, I.; Liz-Marzàn, L. M.; Mulvaney, P. Gold nanorods: synthesis, characterization and applications. *Coord. Chem. Rev.* **2005**, *249*, 1870−1901.
(6) Maier, S. A.; Kik, P. G.; Atwater, H. A.; S. Meltzer, S.; Harel, E.; Koel, B. E.; Requicha, A. A. G. Local detection of electromagnetic energy transport below the diffraction limit in metal nanoparticle plasmon waveguides. *Nat. Mater.* **2003**, *2*, 229−232.
(7) Tabor, C.; Van Haute, D.; El-Sayed, M. A. Effect of orientation on plasmonic coupling between gold nanorods. *ACS Nano* **2009**, *3*, 3670−3678.
(8) Liu, A. Towards development of chemosensors and biosensors with metal-oxide-based nanowires or nanotubes. *Biosens. Bioelectron.* **2008**, *24*, 167−177.
(9) Jackson, J. B.; Halas, N. J. Surface-enhanced Raman scattering on tunable plasmonic nanoparticle substrates. *Proc. Natl. Acad. Sci. U.S.A.* **2004**, *101*, 17930−17935.
(10) Hutchison, J. A.; Centeno, S. P.; Odaka, H.; Fukumura, H.; Hofkens, J.; Uji-i, H. Subdiffraction limited, remote excitation of surface enhanced Raman scattering. *Nano Lett.* **2009**, *9*, 995−1001.
(11) Lal, S.; Link, S.; Halas, N. J. Nano-optics from sensing to waveguiding. *Nat. Photonics* **2007**, *1*, 641−648.
(12) Marhaba, S.; Bachelier, G.; Bonnet, C.; Broyer, M.; Cottancin, E.; Grillet, N.; Lerme, J.; Vialle, J.-L.; Pellarin, M. Surface plasmon resonance of single gold nanodimers near the conductive contact limit. *J. Phys. Chem. C* **2009**, *113*, 4349−4356.
(13) Odom, T. W.; Schatz, G. C. Introduction to plasmonics. *Chem. Rev.* **2011**, *111*, 3667−3668.
(14) Lim, D. K.; Jeon, K. S.; Kim, H. M.; Nam, J. M.; Suh, J. D. Nanogap-engineerable Raman-active nanodumbbells for single-molecule detection. *Nat. Mater.* **2010**, *9*, 60−67.
(15) Jain, P. K.; El-Sayed, M. A. Plasmonic coupling in noble metal nanostructures. *Chem. Phys. Lett.* **2010**, *487*, 153−164.
(16) Marinica, D. C.; Kazansky, A. K.; Nordlander, P.; Aizpurua, J.; Borisov, A. G. Quantum plasmonics: nonlinear effects in the field enhancement of a plasmonic nanoparticle dimer. *Nano Lett.* **2012**, *12*, 1333−1339.
(17) Halas, N. J.; Lal, S.; Chang, W.-S.; Link, S.; Nordlander, P. Plasmons in strongly coupled metallic nanostructures. *Chem. Rev.* **2011**, *111*, 3913−3961.
(18) Grigorenko, I.; Haas, S.; Levi, A. F. J. Electromagnetic response of broken-symmetry nanoscale clusters. *Phys. Rev. Lett.* **2006**, *97*, 036806.
(19) Moon, C. R.; Mattos, L. S.; Foster, B. K.; Zeltzer, G.; Ko, W.; Manoharan, C. H. Quantum phase extraction in isospectral electronic nanostructures. *Science* **2008**, *319*, 782−787.
(20) Gonze, X.; Amadon, B.; Anglade, P. M.; Beuken, J. M.; Bottin, F.; Boulangera, P.; Bruneval, F.; Calistej, D.; Caracas, R.; Coteo, M.; Deutsch, T.; Genovese, L.; Ghosez, Ph.; Giantomassi, M.; Goedeckerc, S.; Hamannm, D. R.; Hermetp, P.; Jollet, F.; Jomard, G.; Leroux, S.; Mancini, M.; Mazevet, S.; Oliveira, M. J. T.; Onida, G.; Pouillon, Y.; Rangel, T.; Rignanese, G. M.; Sangalli, D.; Shaltaf, R.; Torrent, M.; Verstraete, M. J.; Zerahd, G.; Zwanziger, J. W. ABINIT: first-principles approach to material and nanosystem properties. *Comput. Phys. Commun.* **2009**, *180*, 2582−2615.
(21) Marini, A.; Hogan, C.; Grüning, M.; Varsano, D. yambo: an ab initio tool for excited state calculations. *Comput. Phys. Commun.* **2009**, *180*, 1392−1403.
(22) Marini, A.; Onida, G.; Del Sole, R. Plane-wave DFT-LDA calculation of the electronic structure and absorption spectrum of copper. *Phys. Rev. B* **2001**, *64*, 195125.
(23) Durante, N.; Fortunelli, A.; Broyer, M.; Stener, M. Optical properties of Au nanoclusters from TD-DFT calculations. *J. Phys. Chem. C* **2011**, *115*, 6277−6282.
(24) Johnson, H. E.; Aikens, C. Electronic structure and TDDFT optical absorption spectra of silver nanorods. *J. Phys. Chem. A* **2009**, *113*, 4445−4450.
(25) Liao, M.-S.; Bonifassi, P.; Leszczynski, J.; Ray, P. C.; Huang, M.-J.; Watts, J. D. Structure, bonding, and linear optical properties of a series of silver and gold nanorod clusters: DFT/TDDFT studies. *J. Phys. Chem. A* **2010**, *114*, 12701−12708.
(26) Piccini, G.; Havenith, R. W. A.; Broer, R.; Stener, M. Gold nanowires: a time-dependent density functional assessment of plasmonic behavior. *J. Phys. Chem. C* **2013**, *117*, 17196−17204.
(27) Yuan, Z.; Gao, S. End and central plasmon resonances in linear atomic chains. *Phys. Rev. Lett.* **2007**, *98*, 216602.
(28) Grosso, G.; Parravicini, G. P. *Solid State Physics*; Academic Press, 2000; p 251.
(29) Onida, G.; Reining, L.; Rubio, A. Electronic excitations: density-functional versus many-body Green's-function approaches. *Rev. Mod. Phys.* **2002**, *74*, 601−659.
(30) Huang, X. H.; El-Sayed, I. H.; Qian, W.; El-Sayed, M. A. Gold nanoparticles propulsion from surface fueled by absorption of femtosecond laser pulse at their surface plasmon resonance. *J. Am. Chem. Soc.* **2006**, *128*, 2115−2120.
(31) Chan, G. H.; Zhao, J.; Hicks, E. M.; Schatz, G. C.; Van Duyne, R. P. Plasmonic properties of copper nanoparticles fabricated by nanosphere lithography. *Nano Lett.* **2007**, *7*, 1947−1952.
(32) Lozovick, Yu. E.; Klyuchnik, A. V. The dielectric function and collective oscillations in inhomogeneous matter. In *The Dielectric Function of Condensed Systems*; Modern Problems in Condensed Matter Science, Vol. *24*, Keldysh, L. V.; Kirzhnitz, D. A.; Maradudin, A. A., Eds.; Elsevier: Amsterdam; 2013; Chapter 5.
(33) Loginov, E.; Gomez, L. F.; Chiang, N.; Halder, A.; Guggemos, N.; Kresin, V. V.; Vilesov, A. F. Photoabsorption of Ag-N(N similar to 6−6000) nanoclusters formed in helium droplets: transition from compact to multicenter aggregation. *Phys. Rev. Lett.* **2011**, *106*, 233401.
(34) Scholl, J. A.; García-Etxarri, A.; Leen Koh, A.; Dionne, J. A. Observation of quantum tunneling between two plasmonic nanoparticles. *Nano Lett.* **2013**, *13*, 564−569.
(35) Malola, S.; Lehtovaara, L.; Enkovaara, J.; Hakkinen, H. Birth of the localized surface plasmon resonance in mono layer-protected gold nanoclusters. *ACS Nano* **2013**, *7*, 10263−10270.
(36) Zuloaga, J.; Prodan, E.; Nordlander, P. Quantum description of the plasmon resonances of a nanoparticle dimer. *Nano Lett.* **2009**, *9*, 887−891.
(37) Zhao, L.; Jensen, L.; Schatz, G. C. Pyridine-Ag-20 cluster: a model system for studying surface-enhanced Raman scattering. *J. Am. Chem. Soc.* **2006**, *128*, 2911−2919.